

3D-QSAR studies of quinoline Schiff bases as enoyl acyl carrier protein reductase inhibitors

Shrinivas D Joshi
Sheshagiri R Dixit
Uttam A More
Devendra Kumar
Tejraj M Aminabhavi
Venkatrao H Kulkarni

Novel Drug Design and Discovery
Laboratory, Department of
Pharmaceutical Chemistry, SET's
College of Pharmacy, Sangolli Rayanna
Nagar, Karnataka, India

Abstract: Nicotinamide adenine dinucleotide reduced-dependent reduction of *trans*-2-enoyl acyl carrier protein (ACP) to yield nicotinamide adenine dinucleotide (NAD⁺) and reduced enoyl thioester-ACP substrate is catalyzed by the enoyl-ACP reductase (ENR) enzyme which is an important enzyme for type II fatty acid synthesis (FAS-II) (PubMed identifier 15139852). It is also a useful object for the discovery of antimicrobial drugs because of its fundamental role in the metabolism. Hence, inhibition of ENR might be a novel approach in developing antitubercular (anti-TB) drugs. Quinolines are the important class of heterocycles found in natural and synthetic products of various kinds. In this paper, docking and three-dimensional quantitative structure–activity relationship (3D-QSAR) (comparative molecular field analysis [CoMFA], comparative molecular similarity indices analysis [CoMSIA], and Topomer CoMFA) studies were performed on a set of quinoline hydrazones. According to docking studies, active site of the enzyme, amino acid residue TYR158, and co-factor NAD⁺ are important in binding with the ligand. Of all the compounds tested, compounds 45 and 46 have shown a docking score of 6.22, while compound 26 has a docking score of 6.09. The CoMFA model with steric and electrostatic field exhibited $q^2=0.617$, $r^2=0.81$; CoMSIA model displayed $q^2=0.631$, $r^2=0.755$; Topomer CoMFA model exhibited $q^2=0.644$, $r^2=0.865$ with a standard error of estimate (SEE) of 0.37. The docking results provided detailed structurally important binding features between quinoline hydrazones and the ENR enzyme. Our findings also provide useful hints and information for designing compounds with improved inhibitory activity.

Keywords: quinoline hydrazones, enoyl-ACP reductase, docking, QSAR: CoMFA, CoMSIA, Topomer CoMFA

Introduction

Tuberculosis (TB), a chronic disease caused by the pathogenic bacterium *Mycobacterium tuberculosis*, is a global health threat and a major cause of death among adults in developing countries. This has resulted in increasing resistance of clinically significant pathogens to antibiotic treatment.¹ Novel antibacterial agents that act specifically with different mechanisms of actions from the current drug therapies provide more hope of fighting these multidrug-resistant organisms.² For fatty acid synthesis (FAS-II), enoyl acyl carrier protein (ACP) reductase is a key enzyme involved in the reduction of nicotinamide adenine dinucleotide reduced (NADH)-dependent, *trans*-2-enoyl ACP to yield NAD⁺ and reduced enoyl thioester-ACP substrate that are important in fatty acid metabolism, which could be a useful target for antimicrobial drug discovery because of its vital role in the metabolic pathway. Additionally, bacterial enoyl-ACP reductase (ENR) chain and structural organization are noticeably different from those of the

Correspondence: Shrinivas D Joshi
Novel Drug Design and Discovery
Laboratory, Department of
Pharmaceutical Chemistry, SET's College
of Pharmacy, Sangolli Rayanna Nagar,
Dharwad 580 002, India
Tel +91 998 615 1953
Fax +91 836 246 7190
Email shrinivasdj@rediffmail.com

mammalian fatty acid biosynthetic enzymes.^{3,4} In an effort to develop novel class of antitubercular (anti-TB) compounds, we have decided to inhibit bacterial FAS-II.

The quinoline nucleus, an important class of heterocycle, is found in many synthetic and natural products that exhibit an ample range of pharmacological activities, such as antiviral,⁵ anticancer,⁶ antibacterial,⁷ antifungal,⁸ antiobesity,⁹ and anti-inflammatory;¹⁰ these can be illustrated by a large number of drugs in the market having a quinoline structure. However, despite its wide range of pharmacological activities, only a handful of studies have evaluated TB compared to other classes of drugs. Sirturo™/Bedaquiline (TMC 207, Janssen Therapeutics, Titusville, NJ, USA) is a well known anti-TB drug containing diaryl quinoline moiety. It is certainly the first anti-TB drug to interfere with the bacterial energy metabolism by inhibiting mycobacterial ATP (adenosine 5'-triphosphate) synthase, an essential enzyme for the generation of energy in *M. tuberculosis*. Hydrazones (Schiff bases), characterized by the presence of azomethine linkage ($-N=CH-$), play an important role in biological activities such as antibacterial, anti-cestode, antiviral, antitumoral, and anti-TB properties.¹¹⁻²⁰

The docking study reveals structural features required for ligand binding with amino acid residues and the co-factor NAD^+ present in the active site of the enzyme. Quantitative structure-activity relationships (QSAR) are therefore as vital in drug design and discovery studies as ligand-based approaches. Three-dimensional QSAR (3D-QSAR) study is a common method of computer-aided molecular design.²¹ Among these methods, comparative molecular field analysis (CoMFA), proposed by Cramer et al,²¹ has been widely used in drug discovery research that provides a region of steric and electrostatic fields that are essential for biological activity. In a similar manner, the comparative molecular similarity indices analysis (CoMSIA) uses a probe atom to calculate similarity indices at frequently spaced grid points for aligned molecules. The CoMSIA differs from CoMFA initially in the manner in which molecular fields are calculated using a Gaussian-type distance-dependent function to measure five fields of physicochemical properties (electrostatic, steric, hydrophobic, H-bond acceptor, and donor).^{22,23}

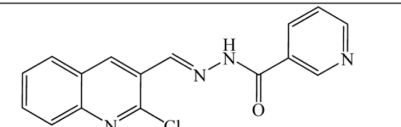
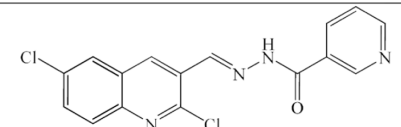
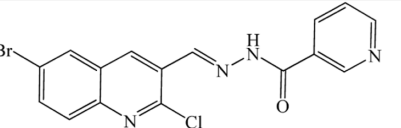
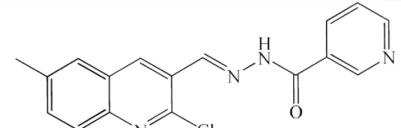
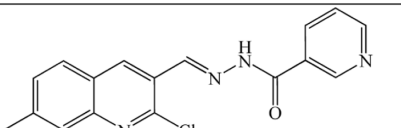
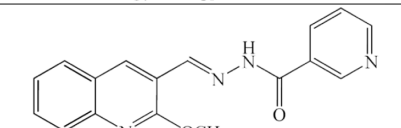
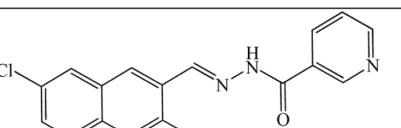
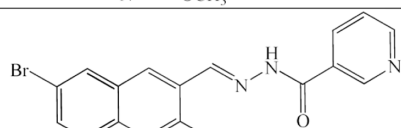
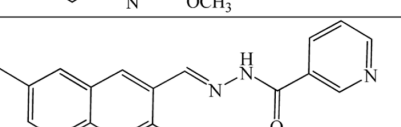
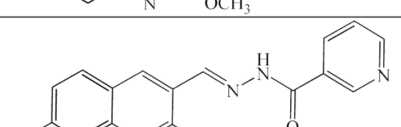
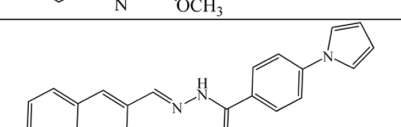
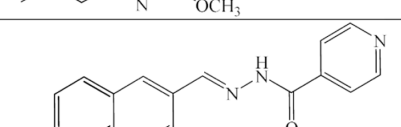
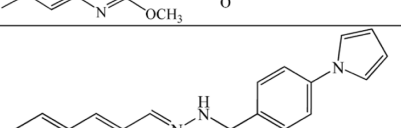
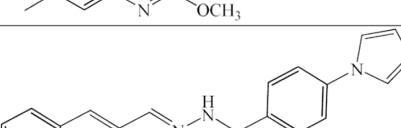
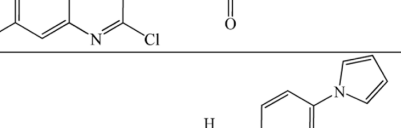
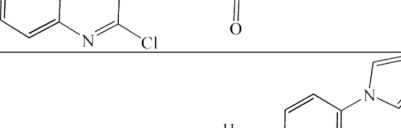
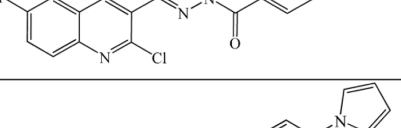
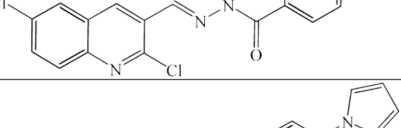
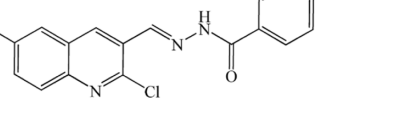
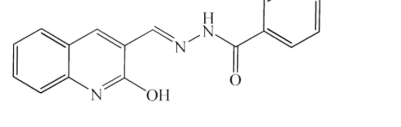
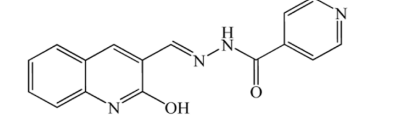
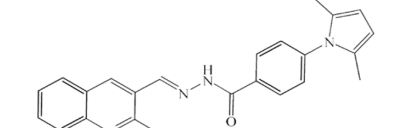
Among the important class of pharmacophores responsible for anti-TB activity, quinoline scaffolds are

Table I Structures and antitubercular activity ($\mu\text{g/mL}$) of Schiff bases of quinoline derivatives (1-75) used for training and test sets

Compound	Structure	MIC	Compound	Structure	MIC
1		1.6	2		1.6
3		0.8	4		1.6
5		0.4	6		0.8
7		0.2	8		0.2
9		0.4	10		0.2

(Continued)

Table I (Continued)

11		3.125	12		1.6
13*		1.6	14		3.125
15		3.125	16		3.125
17*		1.6	18		0.8
19		0.8	20		0.8
21*		0.4	22		0.8
23*		1.6	24		3.125
25		1.6	26		0.8
27		3.125	28		50
29		100	30		6.25
31*		25	32		50

(Continued)

Table I (Continued)

33		100	34		6.25
35		12.5	36*		100
37		6.25	38*		16.4
39		9.8	40		5.3
41		2.7	42		9.7
43		4.9	44		11.8
45		0.6	46		0.6
47		9.5	48		9.5
49*		2.2	50		9.7
51		19.5	52*		4.6
53		4.6	54*		9.0
55		10.2	56		2.4

(Continued)

Table I (Continued)

57		19.5	58		4.8
59		4.8	60		9.4
61		11.3	62*		19.5
63*		4.8	64		9.3
65		4.7	66		9.1
67		4.8	68		2.6
69		9.3	70		9.3
71		4.5	72*		19.3
73		4.0	74*		10.6
75*		5.3			

Notes: *indicates test set.

considered to be the viable lead structures for the design and synthesis of more effective and broad spectrum anti-TB agents. Our previous reports described docking studies on quinoline hydrazones,²⁴ viz, pyrrolyl 1,3,4-oxadiazoles, phthalazine/pyridazines, and pyrrolyl Schiff bases as well as 2D and 3D-QSAR studies on pyrrole derivatives as ENR inhibitors.²⁵⁻²⁸ In continuation of these studies, herein we report docking and 3D-QSAR studies on quinoline hydrazones as anti-TB agents.

Materials and methods

Data set

The data set used in this study contains 75 inhibitors of ENR, which were taken from our reported data^{24,29,30} as well as from the literature³¹ along with their *in vitro* anti-TB activity results expressed in $\mu\text{g/mL}$ (minimum inhibitory concentration [MIC]). The data set was split into a training set (by considering 75% of the total molecules) and a test set (25% in the test set of the total molecules) using the

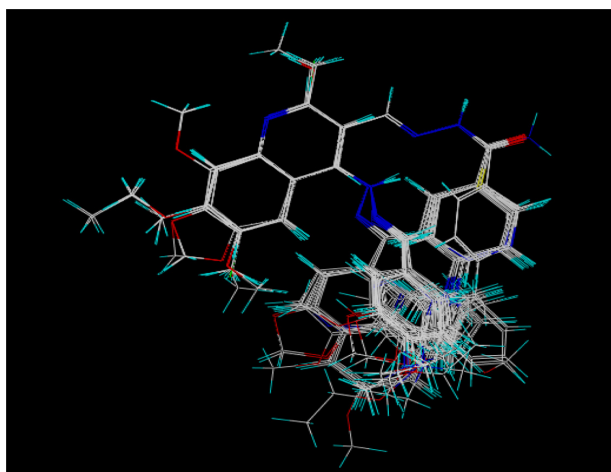


Figure 1 Database alignment of the 75 studied molecules.

diversity method. For the generation of the test and training set, we have used the chemical diversity method. The training set was used to produce 3D-QSAR models, while the test set was used to validate the quality of the model. The chemical structures and biological data for the complete set of compounds are depicted in Table 1.

Molecular modeling and database alignment

The 3D structures of the quinoline scaffold were constructed using standard geometric parameters of molecular modeling software package SYBYL-X 2.0 (Tripos International, St Louis, MO, USA). The use of a reasonably low energy conformation in the alignment is necessary for the statistical evaluation of flexible structures within the CoMFA model. In this study, the structure of each of the 75 quinoline scaffold compounds was geometrically optimized using a standard Tripos molecular mechanics force field with a distance-dependent ($1/r$) dielectric function and energy gradient convergence criterion of 0.05 kcal/mol. In addition, partial atomic charges required for the estimation of electrostatic potential were assigned by Gasteiger–Hückel. The molecule was heated up to 1,000 K within 2,000 fs, held at this temperature for 2,000 fs and annealed to 0 K for 10,000 fs using an exponential annealing function. By applying this procedure, a total of 100 conformations were sampled out during the 100 cycles to account for the conformational flexibility to find the most likely conformation occurring most often in the resulting pool. All the conformations were then minimized using Gasteiger–Hückel charges for all the molecules. Both *cis* and *trans* conformations were analyzed, of which *cis* conformation showed better interaction with the ENR compared to *trans* conformations; also, alignment of *cis* conformations with the ligand was better than *trans*

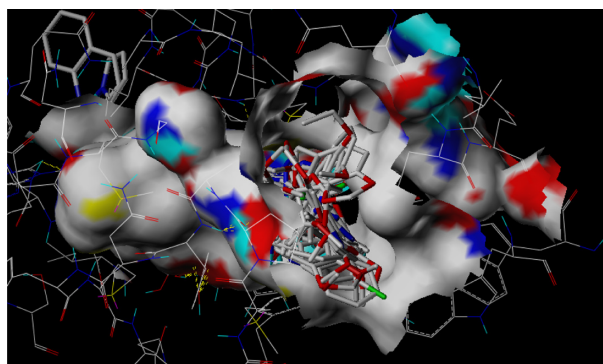


Figure 2 All molecules are docked into the active site of the enzyme.

conformations. All the structures used were aligned into a lattice box by fitting with the quinoline hydrazone as a common structure using compound 7 as a template, because it has the minimum energy conformation with the highest activity and this compound also showed conformational alignment with the ligand (PT70) molecule.²⁴ Figure 1 shows the alignment of all 75 quinoline hydrazones used in this study.

Molecular docking

Surflex docking was carried out on the crystal structure of *M. tuberculosis* InhA inhibited by PT70 which were downloaded from the Protein Data Bank (PDB entry code 2X22, A chain) using the same docking procedure as described previously.²⁴ The binding of quinoline derivatives was anticipated using an array of scoring functions that have been compiled into a single consensus score.

CoMFA and CoMSIA setup

In drug design and discovery, CoMFA and 3D-QSAR techniques are the most widely used computational tools,²¹ since they are capable of predicting biological activity of novel compounds by establishing the relationship between steric/electrostatic properties and biological activities in the form of contour maps. In the present work, ligands are placed in a 3D lattice and then steric as well as electrostatic fields of the ligands at various grid points of the lattice are calculated. The resulting field matrix is then analyzed by the partial least squares (PLS) method.

CoMSIA is one of the newer 3D-QSAR approaches with steric and electrostatic features. Apart from this, it also calculates H-bond donor, H-bond acceptor, and hydrophobic interactions. The CoMSIA similarity indices properties were calculated using a probe with a radius of 1.0 Å and a default value of 0.3 as the attenuation factor. A grid spacing of 2 Å was used for both CoMFA and CoMSIA. The q^2 were calculated using:

Table 2 Surflex docking scores (kcal/mol) of quinoline hydrazones

Compound	Actual pMIC	CScore	
		Predicted pMIC	Δ^a
1	5.79	8.18	-2.39
2	5.79	8.80	-3.01
3	6.09	6.67	-0.58
4	5.79	8.01	-2.21
5	6.39	7.23	-0.84
6	6.09	8.93	-2.84
7	6.69	9.50	-2.81
8	6.69	8.44	-1.75
9	6.39	9.54	-3.15
10	6.69	9.47	-2.78
11	5.50	5.50	0.0
12	5.79	4.39	1.4
13	5.79	5.39	0.4
14	5.50	4.55	0.95
15	5.50	5.10	0.4
16	5.50	6.40	-0.9
17	5.79	5.29	0.5
18	6.09	4.45	1.64
19	6.09	3.96	2.13
20	6.09	6.26	-0.17
21	6.39	7.26	-0.87
22	6.09	5.99	0.1
23	5.79	6.04	-0.25
24	5.50	5.25	0.25
25	5.79	5.30	0.49
26	6.09	4.80	1.29
27	5.50	5.20	0.3
28	4.30	3.50	0.8
29	4.00	3.55	0.45
30	5.20	4.95	0.25
31	4.60	3.86	0.74
32	4.30	3.52	0.78
33	4.00	3.52	0.48
34	5.20	4.88	0.32
35	4.90	5.28	-0.38
36	4.00	3.48	0.52
37	5.20	4.79	0.41
38	4.78	3.93	0.85
39	5.00	5.01	-0.01
40	5.27	6.05	-0.78
41	5.56	7.80	-2.24
42	5.01	5.40	-0.39
43	5.31	6.35	-1.04
44	4.92	4.55	0.37
45	6.22	8.40	-2.18
46	6.22	9.09	-2.87
47	5.02	5.45	-0.43
48	5.02	5.45	-0.43
49	5.65	8.18	-2.53
50	5.01	5.40	-0.39
51	4.71	4.34	0.37
52	5.33	7.33	-2
53	5.33	6.25	-0.92

(Continued)

Table 2 (Continued)

Compound	Actual pMIC	CScore	
		Predicted pMIC	Δ^a
54	5.04	5.62	-0.58
55	4.99	5.10	-0.11
56	5.62	7.86	-2.24
57	4.71	4.32	0.39
58	5.31	6.57	-1.26
59	5.31	6.88	-1.57
60	5.02	5.56	-0.54
61	4.94	4.67	0.27
62	4.71	4.32	0.39
63	5.31	7.02	-1.71
64	5.03	5.48	-0.45
65	5.32	7.25	-1.93
66	5.04	5.57	-0.53
67	5.31	7.34	-2.03
68	5.58	7.78	-2.2
69	5.03	5.73	-0.7
70	5.03	5.75	-0.72
71	5.34	6.35	-1.01
72	4.71	5.95	-1.24
73	5.39	7.50	-2.11
74	4.97	4.99	-0.02
75	5.27	6.06	-0.79
-	-	-	-

Notes: ^aThe difference between experimental and total score values.**Abbreviations:** CScore, consensus score; pMIC, -log minimum inhibitory concentration.

$$q^2 = 1 - \frac{\sum_y (Y_{\text{pred}} - Y_{\text{actual}})^2}{\sum_y (Y_{\text{actual}} - Y_{\text{mean}})^2} \quad (1)$$

where Y_{pred} is the predicted activity, Y_{actual} is the experimental activity, and Y_{mean} is the best estimate of the mean. Then, standard error of estimate (SEE) or SEP was calculated as:

$$\text{SEE, SEP} = \sqrt{\frac{\text{PRESS}}{n - c - 1}} \quad (2)$$

where n is the number of compounds, c is the number of components and the value of PRESS was calculated as:

$$\text{PRESS} = \sum_y (Y_{\text{pred}} - Y_{\text{actual}})^2 \quad (3)$$

Similarity index $A_{F,k}$ for a molecule j with atoms at the grid point q was calculated as:

$$A_{F,k}^q = -\sum_{\text{probe},k} \omega_{\text{probe},k} \omega_{ik} e^{-\alpha r_{iq}^2} \quad (4)$$

where $\omega_{\text{probe},k}$ is the probe atom with radius 1 Å, charge +1, hydrophobicity +1, H-bond donating +1 and H-bond accepting +1; ω_{ik} is the actual value of the physicochemical property k of

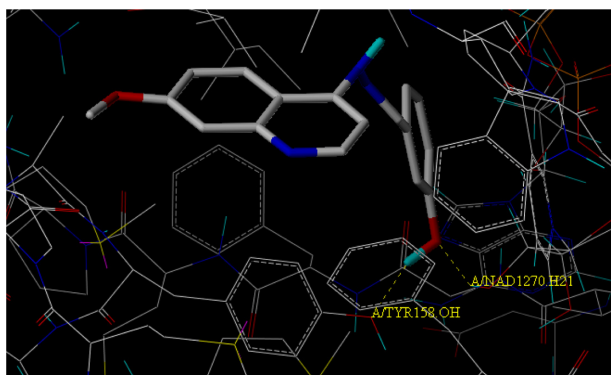


Figure 3 Interaction of compound 40 with the crystal structure of enzyme PDB 2X22.

Abbreviation: PDB, Protein Data Bank.

atom i ; r_{iq} is the mutual distance between the probe atom at grid point q and atom i of the test molecule; α is the attenuation factor, while the default value is 0.3. Five physicochemical properties, viz., k (steric, electrostatic, hydrophobic, H-bond acceptor, and donor) were evaluated using a common charged, hydrophobic and H-bond accepting probe atom.

Topomer CoMFA

A topomer CoMFA technique merges CoMFA and topomer tools to overcome the alignment problem³² of CoMFA. It includes the alignment of structural fragments, which by definition, contains a common characteristic feature – the “open valence” or “attachment bond”. Database alignment was used to produce the CoMFA model, for which each structure of data set was broken into R_1 and R_2 fragments. Once the fragmentation was completed, topomers were automatically standardized, normalized, and generated.

All the aligned compounds or topomers were then placed in a 3D cubic lattice with a grid spacing of 2 Å in

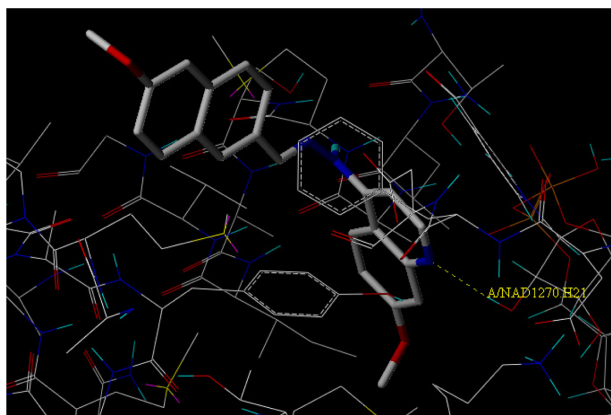


Figure 4 Interaction of compound 46 with the crystal structure of enzyme PDB 2X22.

Abbreviation: PDB, Protein Data Bank.

x , y , and z directions; steric and electrostatic fields were measured for all the compounds or topomers at grid points by the sp^3 hybrid carbon atom with a +1 charge. A default value of 30 kcal/mol was used as an energy cut-off point to minimize the domination by large steric and electrostatic fields for generating CoMFA columns. The 3D-QSAR models were represented as the contour plots of variations in molecular fields (standard deviation of steric or electrostatic field at each grid point) multiplied by the standard deviation*coefficient field.

PLS analysis

PLS analysis provides a correlation between anti-TB activity of the compounds with the predictive values of CoMFA, CoMSIA, and Topomer CoMFA containing a magnitude of steric, electrostatic, hydrophobic potentials, H-bond donor, and acceptor. This regression method was used to analyze the training set by correlating dependent variable values (anti-TB activity) with variations in their independent variables (CoMFA/CoMSIA interaction fields). The optimal number of components was determined with samples-distance partial least square.³³ In order to get the optimal number of elements leading to the highest cross-validated coefficient, q^2 leave-one-out method was used, and SEP, which indicates the reliability and predictive ability of the models, was calculated. The final PLS regression analysis was then obtained from the non-cross-validation method, with the explained difference, r^2 SEE and F ratio. The SEE determines that target improbability property is still unexplained after the model has been derived, and F is the ratio of r^2 to $1-r^2$ weighted factor such that the fewer the explanatory properties and higher the values of the target property, higher will be the F -ratio. The model with an optimum number of components (highest q^2) and with the lowest SEP was selected for further analysis.

The bootstrapping procedure³⁴ was also used to validate each model. In this procedure, n number of random selections out of the training set of n objects were performed a number of times to replicate different samplings from the larger set of objects. In each run, some objects may not be included in the PLS analysis, and some may have been included more than once.

Results and discussion

Molecular docking

The docking study for compounds 1–23 has been reported before,²⁴ while the remaining 52 compounds were docked on the same 2X22 Protein Data Bank file and results of the newly docked compounds are displayed in Figure 2,

Table 3 Actual and predictive activities (pMIC) with residual values (Δ) for the training and test set compounds for CoMFA, CoMSIA and Topomer CoMFA models

Compounds	Actual pMIC	CoMFA		CoMSIA		Topomer CoMFA			
		Predicted pMIC	Δ^a	Predicted pMIC	Δ^a	R ₁	R ₂	Predicted pMIC	Δ^a
1	5.79	5.94	-0.15	6.02	-0.23	0.78	0.23	5.82	-0.03
2	5.79	6.13	-0.33	6.22	-0.43	1.21	0.23	6.24	-0.45
3	6.09	6.13	-0.03	6.28	-0.18	1.15	0.23	6.19	-0.1
4	5.79	5.63	0.15	6.02	-0.22	0.86	0.23	5.89	-0.1
5	6.39	6.31	0.08	6.09	0.30	1.29	0.23	6.32	0.07
6	6.09	6.48	-0.38	6.25	-0.16	1.14	0.23	6.18	-0.09
7	6.69	6.57	0.12	6.42	0.27	1.56	0.23	6.59	0.1
8	6.69	6.65	0.04	6.48	0.21	1.52	0.23	6.56	0.13
9	6.39	6.37	0.02	6.23	0.16	1.19	0.23	6.22	0.17
10	6.69	6.79	-0.09	6.31	0.38	1.68	0.23	6.71	-0.02
11	5.50	5.48	0.02	5.66	-0.16	0.78	-0.15	5.43	0.07
12	5.79	5.63	0.16	5.83	-0.04	1.21	-0.15	5.86	-0.07
13*	5.79	5.60	0.19	5.89	-0.09	1.15	-0.15	5.80	-0.01
14	5.50	5.57	-0.06	5.68	-0.18	0.86	-0.15	5.50	0.00
15	5.50	5.71	-0.21	5.75	-0.24	1.29	-0.15	5.93	-0.43
16	5.50	5.53	-0.02	5.89	-0.39	1.14	-0.15	5.79	-0.29
17*	5.79	5.69	0.10	6.07	-0.27	1.56	-0.15	6.20	-0.41
18	6.09	5.69	0.4	6.12	-0.03	1.52	-0.15	6.17	-0.08
19	6.09	5.65	0.44	5.91	0.18	1.19	-0.15	5.84	0.25
20	6.09	5.90	0.19	5.99	0.10	1.68	-0.15	6.32	-0.23
21*	6.39	6.76	-0.36	6.11	0.28	1.68	-0.30	6.18	0.21
22	6.09	5.44	0.64	5.84	0.25	1.68	-0.77	5.71	0.38
23*	5.79	6.14	-0.34	5.83	-0.03	1.29	-0.30	5.79	0.00
24	5.50	5.66	-0.15	5.73	-0.23	0.78	-0.30	5.29	0.21
25	5.79	5.90	-0.11	5.97	-0.17	1.15	-0.30	5.66	0.13
26	6.09	5.89	0.19	5.91	0.18	1.21	-0.30	5.71	0.38
27	5.50	5.03	0.47	5.69	-0.19	0.86	-0.30	5.36	0.14
28	4.30	4.52	-0.22	4.48	-0.18	0.10	-0.30	4.61	-0.31
29	4.00	4.38	-0.38	4.41	-0.41	0.10	-0.77	4.13	-0.31
30	5.20	4.79	0.40	4.75	0.45	0.10	0.23	5.14	0.06
31*	4.60	4.83	-0.23	4.55	0.05	0.10	-0.15	4.75	-0.15
32	4.30	4.48	-0.18	4.48	-0.18	0.08	-0.30	4.59	-0.29
33	4.00	4.52	-0.52	4.42	-0.42	0.08	-0.77	4.11	-0.11
34	5.20	4.96	0.24	4.78	0.41	0.08	0.23	5.12	0.08
35	4.90	4.95	-0.05	4.55	0.34	0.08	-0.15	4.73	0.17
36*	4.00	4.84	-0.84	4.51	-0.51	0.10	0.11	5.02	-1.02
37	5.20	4.97	0.23	4.52	0.68	0.08	0.11	5.00	0.2
38*	4.78	5.33	-0.55	5.24	-0.43	0.04	0.31	5.15	-0.37
39	5.00	5.04	-0.03	5.19	-0.18	-0.10	0.31	5.01	-0.01
40	5.27	5.29	-0.01	5.27	-0.005	0.09	0.31	5.19	0.08
41	5.56	5.33	0.23	5.35	0.21	0.29	0.31	5.39	0.17
42	5.01	5.42	-0.41	5.24	-0.22	0.18	0.31	5.29	-0.28
43	5.31	5.24	0.06	5.20	0.10	-0.09	0.31	5.01	0.3
44	4.92	4.96	-0.03	5.05	-0.13	0.04	0.31	5.14	-0.22
45	6.22	5.88	0.33	5.34	0.87	0.56	0.31	5.67	0.55
46	6.22	6.12	0.09	5.40	0.81	1.26	0.31	6.37	-0.15
47	5.02	5.86	-0.83	5.35	-0.32	0.50	0.31	5.61	-0.59
48	5.02	5.39	-0.37	5.29	-0.27	0.25	0.31	5.35	-0.33
49*	5.65	5.43	0.22	5.35	0.3	0.26	0.31	5.37	0.28
50	5.01	5.03	-0.02	5.21	-0.19	-0.10	0.29	5.00	0.01
51	4.71	5.07	-0.36	5.19	-0.48	-0.10	0.23	4.93	-0.22
52*	5.33	5.88	-0.54	5.35	-0.01	0.50	0.23	5.53	-0.2

(Continued)

Table 3 (Continued)

Compounds	Actual pMIC	CoMFA		CoMSIA		Topomer CoMFA			
		Predicted pMIC	Δ^a	Predicted pMIC	Δ^a	R ₁	R ₂	Predicted pMIC	Δ^a
53	5.33	5.40	-0.06	5.29	0.03	0.25	0.23	5.28	0.05
54*	5.04	5.44	-0.39	5.24	-0.20	0.18	0.22	5.20	-0.16
55	4.99	5.27	-0.28	5.10	-0.28	-0.10	0.34	5.05	-0.06
56	5.62	5.28	0.34	5.18	0.43	0.18	0.34	5.32	0.3
57	4.71	4.89	-0.18	5.10	-0.39	-0.09	0.34	5.05	-0.34
58	5.31	5.21	0.10	5.17	0.14	-0.10	0.28	4.99	0.32
59	5.31	5.26	0.05	5.19	0.12	0.18	0.28	5.26	0.05
60	5.02	4.88	0.14	5.14	-0.11	-0.09	0.28	4.99	0.03
61	4.94	4.90	0.03	5.20	-0.26	0.04	0.10	4.94	0.00
62*	4.71	4.52	0.18	5.18	-0.47	-0.09	0.10	4.80	-0.09
63*	5.31	5.24	0.07	5.17	0.14	0.54	0.10	5.44	-0.13
64	5.03	4.81	0.21	5.15	-0.11	0.16	0.01	4.97	0.06
65	5.32	5.26	0.06	5.17	0.15	0.54	0.01	5.35	-0.03
66	5.04	4.80	0.23	5.08	-0.04	0.24	0.01	5.05	-0.01
67	5.31	5.17	0.14	5.23	0.08	-0.10	0.47	5.18	0.13
68	5.58	5.48	0.1	5.28	0.30	0.04	0.39	5.23	0.35
69	5.03	5.20	-0.17	5.23	-0.20	-0.10	0.39	5.09	-0.06
70	5.03	5.36	-0.33	5.31	-0.27	0.14	0.39	5.33	-0.3
71	5.34	5.46	-0.11	5.30	0.04	0.18	0.39	5.37	-0.03
72*	4.71	5.51	-0.79	5.28	-0.57	0.01	0.39	5.20	-0.49
73	5.39	5.21	0.18	5.26	0.13	0.09	0.39	5.28	0.11
74*	4.97	5.19	-0.22	5.21	-0.24	0.04	0.39	5.22	-0.25
75*	5.27	5.11	0.15	5.15	0.11	0.09	0.39	5.28	-0.01

Notes: * Indicates test set. ^aThe difference between experimental and predicted values.

Abbreviations: CoMFA, comparative molecular field analysis; CoMSIA, comparative molecular similarity indices analysis; pMIC, -log minimum inhibitory concentration.

Table 4 PLS statistics of CoMFA, CoMSIA, and Topomer CoMFA model

Statistical parameters	CoMFA	CoMSIA	Topomer CoMFA
q ²	0.617	0.631	0.664
N	4	3	4
r ²	0.810	0.755	0.865
SEE	0.271	0.31	0.37
F	247.471	179.142	370.109
r ² _{pred}	0.890	0.820	0.925
r ² _{LOO}	0.797	0.737	0.857
r ² _{bs}	0.807	0.763	0.850
SD _{bs}	0.057	0.081	0.229

Contour map

Contour	Colour	CoMFA		CoMSIA		Topomer CoMFA			
		Contour level	Volume estimate	Contour level	Volume estimate	R ₁ Contour level	R ₁ Volume estimate	R ₂ Contour level	R ₂ Volume estimate
Steric	Yellow	-0.008	63.1	-0.001	18.3	-0.007	21.7	-0.005	35.8
	Green	0.011	132.8	0.002	94.7	0.020	95.0	0.007	69.5
Electrostatic	Red	-0.017	20.4	-0.004	86.2	-0.009	30.6	-0.005	74.6
	Blue	0.018	20.0	0.005	59.4	0.013	11.0	0.007	26.3
Hydrophobic	White	-	-	-0.003	45.2	-	-	-	-
	Yellow	-	-	0.004	45.3	-	-	-	-
Donor	Purple	-	-	-0.014	41.4	-	-	-	-
	Cyan	-	-	0.006	15.7	-	-	-	-
Acceptor	Red	-	-	-0.005	50.7	-	-	-	-
	Magenta	-	-	0.004	55.0	-	-	-	-

Abbreviations: CoMFA, comparative molecular field analysis; CoMSIA, comparative molecular similarity indices analysis; F, F-test value; N, optimal number of components; PLS, partial least squares; q², leave-one-out; r², non-cross-validation coefficient; r²_{pred}, predictive correlation coefficient; r²_{bs}, mean r² of bootstrapping analysis (100 runs); SEE, standard error of estimation; SD_{bs}, mean standard deviation by bootstrapping analysis.

while the predicted binding energies of the compounds are listed in Table 2. The ligand PT70 (analogue of triclosan) extracted from the enzyme has shown a docking score of 13.48; triclosan used as a standard inhibitor showed²⁵ a docking score of 6.29. Figures 3 and 4 show docking of the highly active compounds 40 and 46 into the active site of ENR. As depicted in Figure 3, compound 46 showed the H-bond interaction between the nitrogen of quinoline moiety and hydrogen of the NAD1270. Compound 40 (Figure 4) has two H-bond interactions, ie, hydrogen of OH interacts with the oxygen of TYR158 and the second interaction occurs between the oxygen of hydroxy group and the hydrogen of NAD1270. Based on the docking score, it may be concluded that the compounds showed good interaction with the enzyme active site compared to triclosan.

3D-QSAR

CoMFA, CoMSIA, and Topomer CoMFA models were developed for a set of 75 inhibitors of ENR. The corresponding values of MIC vary from 0.2 to 100 $\mu\text{g}/\text{mL}$ (Table 1). The *in vitro* MIC values were changed to the corresponding pMIC ($-\log \text{MIC}$) values, but the invention of reliable models is dependent on the formation of appropriate training and test sets. The data set of 75 inhibitors was divided into training (60 compounds) and test (15 compounds) sets (see Table 1). The predictive ability of the models was depicted in Table 3.

The PLS method was used for each of the 3D-QSAR models. The CoMFA, CoMSIA, and Topomer CoMFA values were used as independent variables, whereas pMIC values were used as dependent variables in PLS regression analyses to develop the QSAR models. Predictive ability of the models was assessed by their q^2 values (Table 4).

CoMFA and CoMSIA models

The CoMFA and CoMSIA experiments were performed on molecular modeling software package SYBYL-X 2.0 and molecular atomic charges were calculated using the Gasteiger–Hückel set of rules. The statistical parameters obtained from CoMFA and CoMSIA analyses are shown in Table 4. The best predictions were obtained for the CoMFA model with $q^2=0.617$ ($r^2=0.81$, $\text{SEE}=0.27$, $F=247.471$) and for CoMSIA model $q^2=0.631$ ($r^2=0.755$, $\text{SEE}=0.31$, $F=179.142$) for the selected binding mode. Table 3 shows the CoMFA and CoMSIA predictive values for the training and test set. The plots of predicted versus observed activity values for the training and test set molecules for CoMFA and CoMSIA are shown in Figure 5.

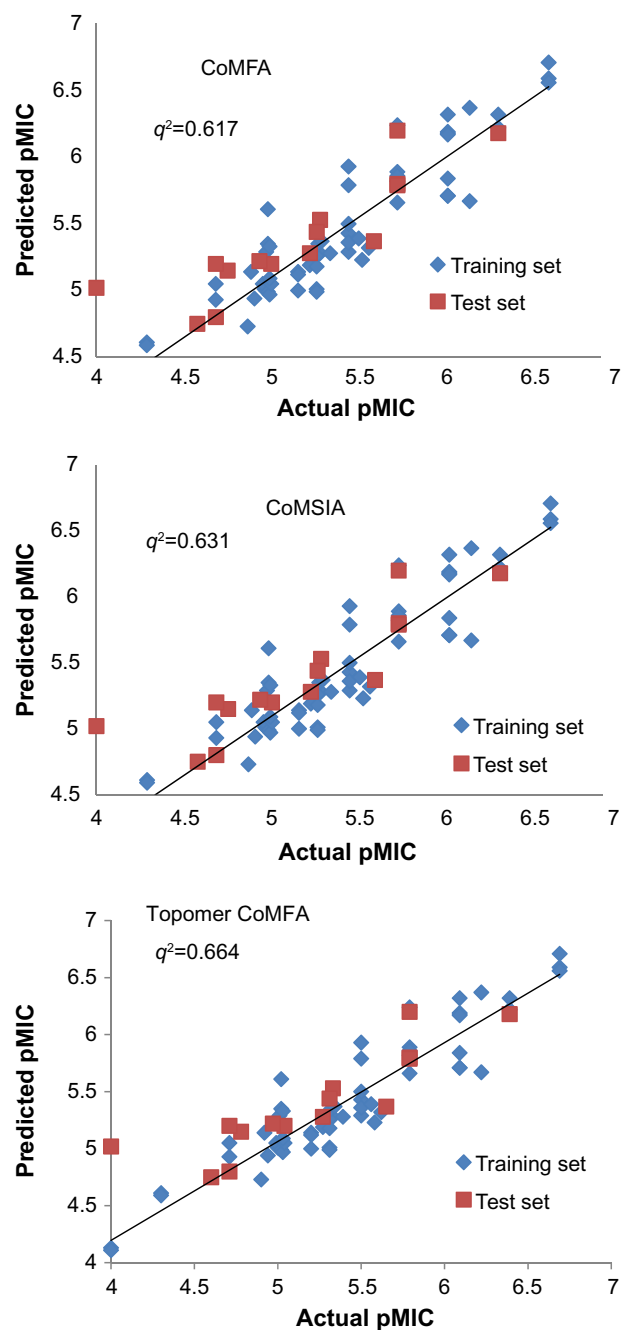


Figure 5 Scatter plot diagram for CoMFA and CoMSIA analysis by database alignment.

Abbreviations: CoMFA, comparative molecular field analysis; CoMSIA, comparative molecular similarity indices analysis; pMIC, $-\log$ minimum inhibitory concentration.

CoMFA and CoMSIA contour map analyses

Three-dimensional contour maps were plotted for CoMFA steric and electrostatic fields from the final non-cross-validated analysis. The field energies at each lattice point were considered as the scalar results of the coefficient and standard deviation associated with a particular column of data table (standard deviation*coefficient of variation)

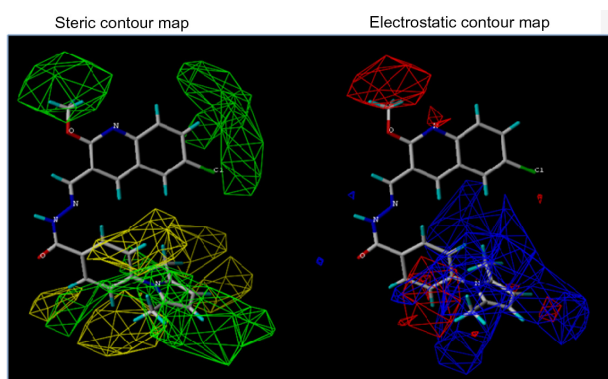


Figure 6 Steric and electrostatic standard deviation*coefficient map for compound 7 by CoMFA analysis.

Notes: Sterically favored/unfavored areas are shown in green/yellow contour, while the blue/red contour depicts the favorable site for positively/negatively charged groups.

Abbreviation: CoMFA, comparative molecular field analysis.

(always plotted as % of contribution of CoMFA equation). The map represents the difference in molecular fields that are associated with the differences in biological activity, which in turn, indicates the place where the aligned molecules would favorably or unfavorably interact with the receptor, while the CoMSIA map indicates that the presence of a specific group at a specified region with a particular physicochemical property will be favored or disfavored for exhibiting good biological activity. The CoMSIA models are easier to interpret because they indicate favorable or unfavorable interaction toward receptors in the form of steric, electrostatic, hydrophobic, H-bond donor, and acceptor compared to the CoMFA models as they only show favorable or unfavorable interaction toward the receptor in the form of steric and electrostatic fields.

Analysis of CoMFA steric (80%) and electrostatic (20%) regions of the contour maps shows green regions near quinoline (C_2 , C_6 , and C_7) and the dimethyl pyrrole ring, which suggests that sterically bulky groups are

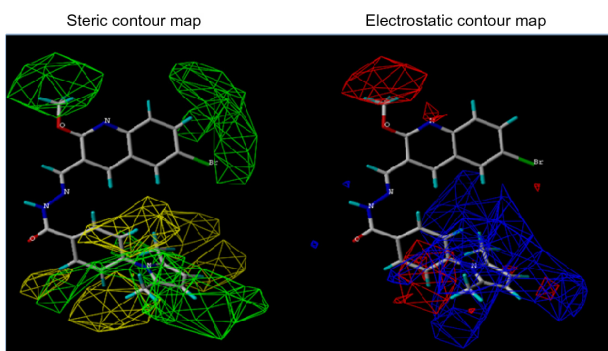


Figure 7 Steric and electrostatic standard deviation*coefficient map for compound 8 by CoMFA analysis.

Notes: Sterically favored/unfavored areas are shown in green/yellow contour, while the blue/red contour depicts the favorable site for positively/negatively charged groups.

Abbreviation: CoMFA, comparative molecular field analysis.

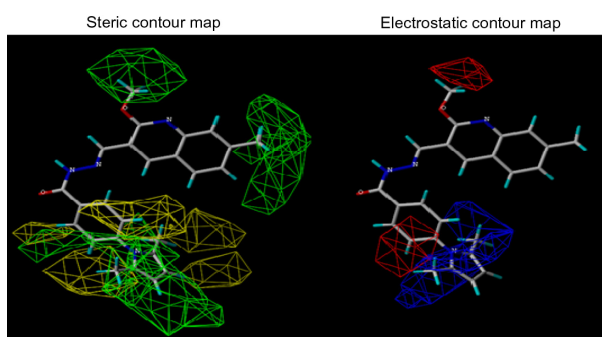


Figure 8 Steric and electrostatic standard deviation*coefficient map for compound 10 by CoMFA analysis.

Notes: Sterically favored/unfavored areas are shown in green/yellow contour, while the blue/red contour depicts the favorable site for positively/negatively charged groups.

Abbreviation: CoMFA, comparative molecular field analysis.

favorable in increasing the activity. As we can see in the contour map of compounds 10 and 9, there is a presence of methyl group at the 6th/7th positions compared to compound 8 containing the bromine atom and compound 7 with the chlorine atom at the 6th position, which shows that the electron donating group is favorable for exhibiting the biological activity. However, a large blue contour around aromatic and dimethyl pyrrole moiety shows the presence of a positively charged group that would increase the activity (Figures 6–9). Contour maps of CoMSIA (steric) (Figure 10A) are almost similar to the subsequent CoMFA region contour maps.

Electrostatic field

The red contour indicates the region with the presence of electron withdrawing groups, and the blue contours indicate the presence of electron donating groups that will enhance the activity. However, the activity of compound 10 (pMIC=6.31) is mainly credited to the presence of the methoxy group, as shown in Figure 10B. Such a contribution is lacking for compounds 27 (pMIC=5.50), 29 (pMIC=4.00), and 51 (pMIC=4.71).

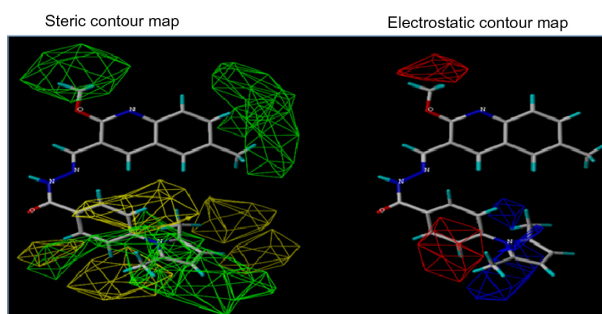


Figure 9 Steric and electrostatic standard deviation*coefficient map for compound 9 by CoMFA analysis.

Notes: Sterically favored/unfavored areas are shown in green/yellow contour, while the blue/red contour depicts the favorable site for positively/negatively charged groups.

Abbreviation: CoMFA, comparative molecular field analysis.

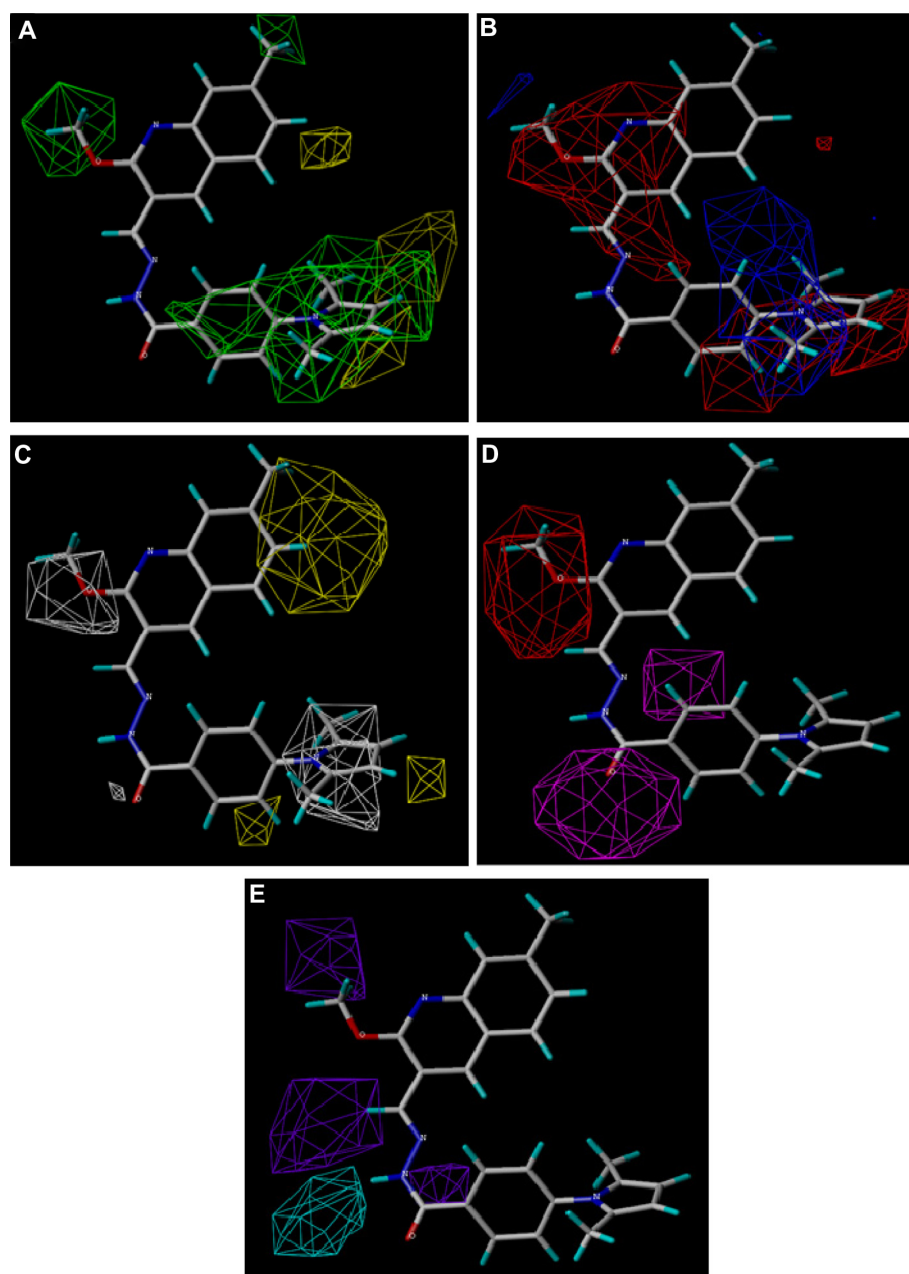


Figure 10 Standard deviation*coefficient contour maps of CoMSIA analysis for compound 10 by database alignment.

Notes: (A) Steric contour map. Green and yellow contours refer to sterically favored and disfavored regions, respectively. (B) Electrostatic contour map. Blue and red contours refer to electronic donating and withdrawing groups in the favored region, respectively. (C) Hydrophobic contour map. White contours refer to the hydrophilic substituent favored region. (D) Hydrogen bond acceptor contour map. The magenta contours for the hydrogen bond acceptor group increase activity, red contours indicate the disfavored region. (E) Hydrogen bond donor contour map. The cyan and purple contours indicate favorable and unfavorable hydrogen bond donor groups, respectively.

Abbreviation: CoMSIA, comparative molecular similarity indices analysis.

Hydrophobic field

According to the CoMSIA model, as shown in Figure 10C, the yellow contour on the aromatic ring represents a favorable region for a hydrophobic substituent, while the O atom of $-OCH_3$ and pyrrole moiety with white contours emphasizes the favoring effect of hydrophilic substituent.

Hydrogen-bond-acceptor field

In Figure 10D, the magenta color in the region of $C=O$ can be observed, indicating aromatic protons favored for the activity.

Hydrogen-bond-donor field

In Figure 10E, it can be observed that the cyan contour near the primary amine group is favored for the activity.

Topomer CoMFA model

Topomer CoMFA was applied on a training set of 60 compounds by splitting into R_1 and R_2 fragments. Compound 7 was used as a template to fragment the training set. The Topomer CoMFA model gives both statistical and graphical results. The statistical parameter gave the predictable

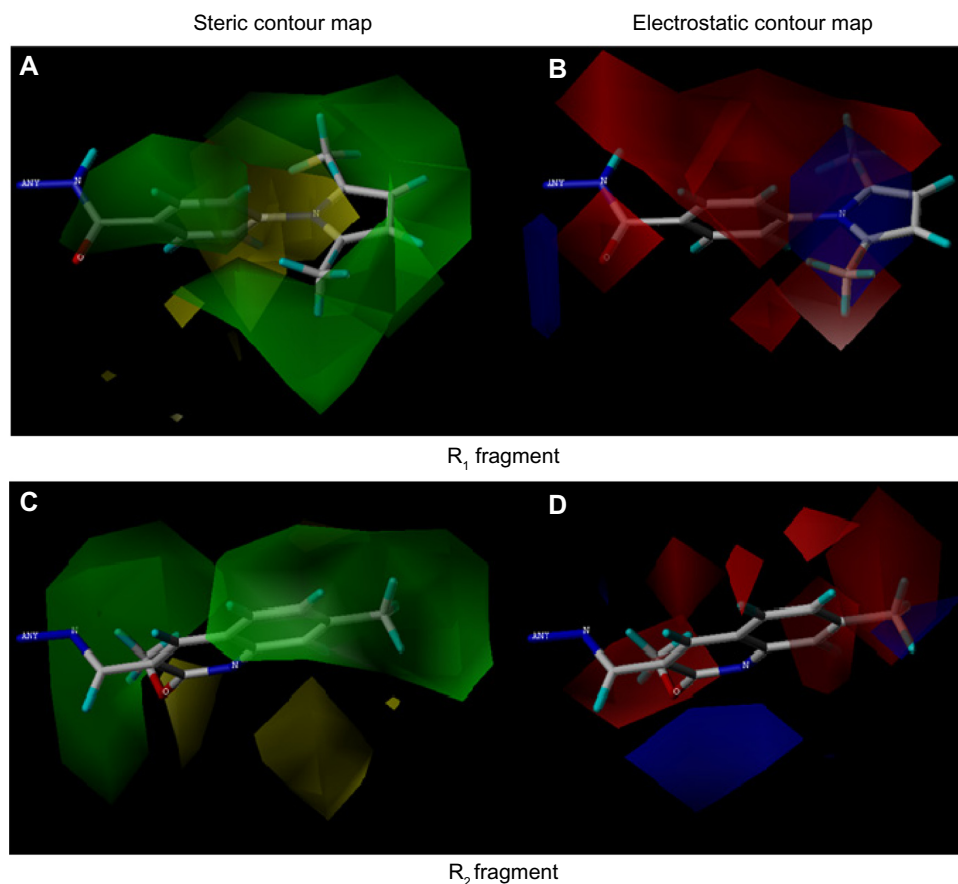


Figure 11 Steric and electrostatic standard deviation*coefficient contour map for compound 10 by Topomer CoMFA analysis.

Notes: (A) Steric contour map for the R₁ fragment. (B) Electrostatic contour map for the R₁ fragment. (C) Steric contour map for the R₂ fragment. (D) Electrostatic contour map for the R₂ fragment. Sterically favored/disfavored region shown in green/yellow contour, while the favorable site for positively/negatively charged groups is shown in blue/red contour.

Abbreviation: CoMFA, comparative molecular field analysis.

non-cross-validated correlation coefficient, r^2 of 0.86 using four PLS components, while the cross-validation gave q^2 of 0.664, $F=370.109$ and r^2_{pred} of 0.865 (Table 4). The predicted activities of the dataset, along with R₁ and R₂ fragment contribution, are shown in Table 3. Plots of predicted versus actual (experimental) activity of the training set and test set molecules are shown in Figure 5.

Graphically, the Topomer CoMFA steric and electrostatic fields for the analysis are represented as contour plots in Figures 11 and 12. The steric contour map displayed in Figure 11A and C showed a broad green contour on the aromatic ring, but pyrrole moiety suggests that substitution of a more bulkier group enhances the potency, while the yellow polyhedral surrounded regions with less bulkier groups enhance the biological activity. The electrostatic contour map shown in Figure 11B and D shows a region of red polyhedron (on the aromatic ring), indicating that electron-rich groups are favorable for exhibiting the activity. Additionally, the blue contour in Figure 11B and D indicates

that the electron withdrawing substituent diminishes the biological activity.

The steric contour map for compound 7 is displayed in Figure 12A and 12C by a big green contour. If a substituent like 4-(2,5-dimethyl-1H-pyrrol-1-yl)benzamide in R₁ fragment and quinoline in R₂ fragment is attached to compound 7 (pMIC =6.59), it occupies the green contour to increase the biological activity. Additionally, the contour plot shows a yellow polyhedron in the bottom right corner of Figure 12C. The yellow contour will slow down the biological activity if a bulky substituent exists, which represents the disfavored steric region. The electrostatic contour map represented in Figure 12B and D shows a region of red polyhedral space, indicating that electron-rich group enhances the activity. Additionally, a blue polyhedron in Figure 12B and D indicates that an electron-rich substituent reduces the biological activity.

Based on the docking and 3D-QSAR studies of all the 75 quinoline scaffolds, we find that in compound 7, there is

and graphical parameters that proved their good predictability of the generated model. This study also proved the presence of $-\text{CH}=\text{N}-$ and quinoline ring that are very much essential for exhibiting the anti-TB activity. Further, the study revealed that compounds are more lipophilic in nature and hence are able to exhibit good biological activities, since *M. tuberculosis* has a high concentration of lipid layer. The reported models may be explored further to design the newer potent compounds with better anti-TB activity.

Acknowledgments

We thank the Council of Scientific and Industrial Research, New Delhi, India (Letter No. 02(0139)/13/EMR-II dated- 12/04/2013) for financial support, and Mr HV Dambal, President, SET's College of Pharmacy, Dharwad, India, for his encouragement. The authors acknowledge Mr SA Tiwari and Mr Ravi N Nadiger for their technical support. One of the authors (Sheshagiri Dixit) thanks Rajiv Gandhi University of Health Sciences, Bangalore, India.

Disclosure

The authors report no conflicts of interest in this work.

References

- Neu HC. The crisis in antibiotic resistance. *Science*. 1992;257(5073):1064–1073.
- Chu DTW, Plattner JJ, Katz L. New directions in antibacterial research. *J Med Chem*. 1996;39(20): 3853–3874.
- Cronan JE. Remarkable structural variation within fatty acid megasynthases. *Nat Chem Biol*. 2006;2(5):232–234.
- Maier T, Jenni S, Ban N. Architecture of mammalian fatty acid synthase at 4.5 Å resolution. *Science*. 2006;311(5765):1258–1262.
- Font M, Monge A, Ruiz I, Heras B. Structure-activity relationships in quinoline Resissert derivatives with HIV-1 reverse transcriptase inhibitory activity. *Drug Des Discov*. 1997;14(4):259–272.
- Nakamura T, Oka M, Aizawa K, et al. Direct interaction between a quinoline derivative, MS-209, and multidrug resistance protein (MRP) in human gastric cancer cells. *Biochem Biophys Res Commun*. 1999;255(3):618–624.
- Kaminsky D, Meltzer RI. Quinolone antibacterial agents. Oxolinic acid and related compounds. *J Med Chem*. 1968;11(1):160–163.
- Musioli R, Jampilek J, Buchta V, et al. Antifungal properties <http://www.sciencedirect.com/science/article/pii/S0968089606000563> of new series of quinoline derivatives. *Bioorg Med Chem*. 2006;14(10):3592–3598.
- Warshakoon NC, Sheville J, Bhatt RT, et al. Design and synthesis of substituted quinolines as novel and selective melanin concentrating hormone antagonists as anti-obesity agents. *Bioorg Med Chem Lett*. 2006;16(19):5207–5211.
- Sloboda AE, Powell D, Poletto JF, Pickett WC, Gibbons JJ Jr, Bell DH, et al. Antiinflammatory and antiarthritic properties of a substituted quinoline carboxylic acid: CL 306,293. *J Rheumatol*. 1991;18(6):855–860.
- Berkoff CE, Craig PN, Gordan BP, Pellerano C. Quinolinehydrazones: structure-activity correlations in a new class of anti-mycoplasmal agents. *Arzneimittelforschung*. 1973;23(6):830–839.
- Actor PP, Pellerano CEG, inventors; SmithKline and French Laboratories, assignee. Anticestode hydrazinoquinolines. United States Patent US 3,646,019. February 29, 1972.
- Pellerano C, Savini L, Berkoff CE, Thomas J, Actor P. Anticestode quinolinehydrazones. *Farmaco Sci*. 1975;30(12):965–973.
- Thomas J, Berkoff CE, Flagg WB, Gallo JJ, Haff RF, Pinto CA. Antiviral quinolinehydrazones. A modified Free-Wilson analysis. *J Med Chem*. 1975;18(3):245–250.
- Bartolucci C, Cellai L, Di Filippo P, et al. Quinolinehydrazones as inhibitors of retroviral reverse transcriptase. *Farmaco*. 1992;47(6): 945–952.
- Pellerano C, Savini L, Massarelli P. [Tridentate N-N-N chelating systems as potential antitumor agents]. *Farmaco Sci*. 1985;40(9): 645–654.
- Savini L, Massarelli P, Chiasserini L, et al. Chelating agents as potential antitumorals. 2-quinolyldhydrazones and bis-2-quinolyldhydrazones. *Eur J Med Chem*. 1995;30(7–8):547–552.
- Savini L, Massarelli P, Chiasserini L, Nencini C, Pellerano C. Chelating agents as potential antitumorals: alpha-(N)-heterocyclic hydrazones and bis-alpha-(N)-heterocyclic hydrazones. *Farmaco*. 1997;52(10):609–613.
- Pellerano C, Savini L, Selvolini L. [Quinolilhydrazones of acetylpyridine: preparation and biological activity. VII]. *Boll Chim Farm*. 1978;117(12):721–730.
- Revanasiddappa BC, Subrahmanyam EVS, Satyanarayana D, Thomas J. Synthesis and biological studies of some novel schiff bases and hydrazones derived from 8-hydroxy quinoline moiety. *Int J Chem Tech Res*. 2009;1(4):1100–1104.
- Cramer RD, Patterson DE, Bunce JD. Comparative molecular field analysis (CoMFA). 1. Effect of shape on binding of steroids to carrier proteins. *J Am Chem Soc*. 1988;110(18):5959–5967.
- Klebe G, Abraham U, Mietzner T. Molecular similarity indices in a comparative molecular field analysis (CoMSIA) of drug molecules to correlate and predict their biological activity. *J Med Chem*. 1994;37(24):4130–4146.
- Ghasemi JB, Pirhadi S, Ayati M. 3D-QSAR studies of 2-arylbenzoxazoles as novel cholesteryl ester transfer protein inhibitors. *Bull Korean Chem Soc*. 2011;32(2):645–650.
- Joshi SD, More UA, Dixit SR, Dubey D, Tripathi A, Kulkarni VH. Discovering potent inhibitors against the enoyl-acyl carrier protein reductase (InhA) of mycobacterium tuberculosis: structure-based design, synthesis and antimicrobial activity of quinoline hydrazones. *Indo Am J Pharm Res*. 2014;4(2):864–877.
- Joshi SD, More UA, Pansuriya K, Aminabhavi TM, Gadad AK. Synthesis and molecular modeling studies of novel pyrrole analogs as antimycobacterial agents. *J Saudi Chem Soc*. In press 2013.
- Joshi SD, More UA, Aminabhavi TM, Badiger AM. Two- and three-dimensional QSAR studies on a set of antimycobacterial pyrroles: CoMFA, Topomer CoMFA, and HQSAR. *Med Chem Res*. 2014;23(1): 107–126.
- Joshi SD, More UA, Dixit SR, Korat HH, Aminabhavi TM, Badiger AM. Synthesis, characterization, biological activity, and 3D-QSAR studies on some novel class of pyrrole derivatives as antitubercular agents. *Med Chem Res*. 2014;23(3):1123–1147.
- More UA, Joshi SD, Aminabhavi TM, Gadad AK, Nadagouda MN, Kulkarni VH. Design, synthesis, molecular docking and 3D-QSAR studies of potent inhibitors of enoyl-acyl carrier protein reductase as potential antimycobacterial agents. *Eur J Med Chem*. 2014;71: 199–218.
- Joshi SD, Joshi A, Vagdevi HM, Vaidya VP, Gadaginamath GS. Microwave assisted synthesis of some new quinolinyl pyrrole derivatives as potential antibacterial and antitubercular agents. *Ind J Heterocycl Chem*. 2010;19:221–224.
- Pradeep Kumar MR, Joshi SD, Dixit SR, Kulkarni VH. Synthesis, antibacterial and antitubercular activities of some novel quinoline derivatives. *Ind J Heterocycl Chem*. 2014;23:353–358.
- Gemma S, Savini L, Altarelli M, et al. Development of antitubercular compounds based on a 4-quinolyldhydrazone scaffold. Further structure-activity relationship studies. *Bioorg Med Chem*. 2009;17(16):6063–6072.

32. Cramer RD. Topomer CoMFA: a design methodology for rapid lead optimization. *J Med Chem.* 2003;46(3):374–388.
33. Bush BL, Nachbar RB Jr. Sample-distance partial least squares: PLS optimized for many variables, with application to CoMFA. *J Comput Aided Mol Des.* 1993;7(5):587–619.
34. Vong R, Geladi P, Wold S, Esbensen K. Source contributions to ambient aerosol calculated by discriminant partial least squares regression (PLS). *J Chemometr.* 1988;2(4):281–296.

Research and Reports in Medicinal Chemistry

Publish your work in this journal

Research and Reports in Medicinal Chemistry is an international, peer-reviewed, open access journal publishing original research, reports, reviews and commentaries on all areas of medicinal chemistry. The manuscript management system is completely online and includes a very quick and fair peer-review system, which is all easy to use.

Submit your manuscript here: <http://www.dovepress.com/research-and-reports-in-medicinal-chemistry-journal>

Dovepress

Visit <http://www.dovepress.com/testimonials.php> to read real quotes from published authors.